Nonlinear Emission of Quinolizinium Based Dyes With Application in Fluorescence Lifetime Imaging.

ARTICLE *in* THE JOURNAL OF PHYSICAL CHEMISTRY A · AUGUST 2014

Impact Factor: 2.69 · DOI: 10.1021/jp507095b · Source: PubMed

THE JOURNAL OF PHYSICAL CHEMISTRY A

Article

pubs.acs.org/JPCA

Nonlinear Emission of Quinolizinium-Based Dyes with Application in Fluorescence Lifetime Imaging

Gema Marcelo,[†,⊥] Sandra Pinto,[†,§] Tatiana Cañeque,[‡] Inês F. A. Mariz,[†] Ana M. Cuadro,[‡] Juan J. Vaquero,[‡] José M. G. Martinho,[†] and Ermelinda M. S. Maçôas*[,†]

[†]Centro de Química-Física Molecular (CQFM) and Institute of Nanoscience and Nanotechnology (IN), Instituto Superior Técnico, Universidade de Lisboa, Av. Rovisco Pais, 1, 1049-001 Lisboa, Portugal

[‡]Departamento de Química Orgánica y Química Inorganica, Universidad de Alcalá, 28871, Alcalá de Henares, Madrid, Spain

[§]Instituto de Medicina Molecular, Faculdade de Medicina, Universidade de Lisboa, Av. Prof. Egas Moniz, 1649-028 Lisbon, Portugal

Supporting Information

ABSTRACT: Charged molecules based on the quinolizinum cation have potential applications as labels in fluorescence imaging in biological media under nonlinear excitation. A systematic study of the linear and nonlinear photophysics of derivatives of the quinolizinum cation substituted by either dimethylaniline or methoxyphenyl electron donors is performed. The effects of donor strength, conjugation length, and symmetry in the two-photon emission efficiency are analyzed in detail. The best performing nonlinear fluorophore, with two-photon absorption cross sections of 1140 GM and an emission quantum yield of 0.22, is characterized by a symmetric D-π-A$^+$-π-D architecture based on the methoxyphenyl substituent. Application of this molecule as a fluorescent marker in optical microscopy of living cells revealed that, under favorable conditions, the fluorophore can be localized in the cytoplasmatic compartment of the cell, staining vesicular shape organelles. At higher dye concentrations and longer staining times, the fluorophore can also penetrate into the nucleus. The nonlinearly excited fluorescence lifetime imaging shows that the fluorophore lifetime is sensitive to its location in the different cell compartments. Using fluorescence lifetime microscopy, a multicolor map of the cell is drafted with a single dye.

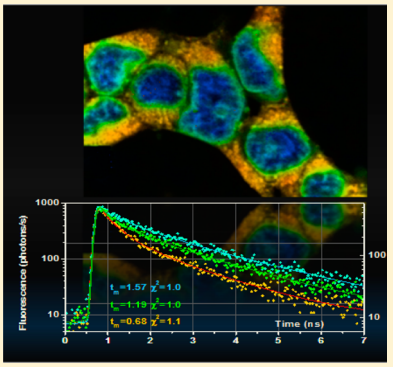

1. INTRODUCTION

Compounds with two-photon excited fluorescence (TPF) are routinely used as markers in in vivo optical microscopy.[1] TPF microscopy can be particularly advantageous in the acquisition of 3D-images owing to the intrinsically reduced out-of-focus photobleaching and photodamage, and the greater penetration depth in biological samples of the longer wavelengths used for multiphoton excitation.[2] In addition, the up-converted emission signal, usually in the visible range, is very efficiently separated from scattered excitation light. The main disadvantage of TPF microscopy relates to the significant bleaching induced in the focal plane by the high excitation power required owing to the low probability of the nonlinear absorption process (typical values of two-photon absorption (TPA) cross sections are $\sigma_2 \approx 10^{-51}$–$10^{-48}$ cm^4 s, while linear absorption cross-section values are $\sigma_1 \approx 10^{-19}$–$10^{-16}$ cm^2). One way to reduce this effect is by designing more efficient TPF fluorophores. Indeed, the commercially available fluorophores used as dyes in bioimaging, which simultaneously show a high degree of selectivity toward specific cell organelles and biologically relevant molecules, have very low TPA cross sections ($\sigma 2$ < 20 GM, 1GM = 10^{-50} cm^4 s), with exceptionally high values around 200 GM reported for a few fluorophores.[3]

Open-shell and charged systems are among the different design strategies that are still challenging and specially promising for future developments of TPF organic dyes.[4] Nevertheless, to the best of our knowledge, only a hand full of cationic systems have been targeted for optimization of the nonlinear optical response together with their application in microscopy of living cells. Examples of this are the wide series of cationic styryl cyanine dyes.[5,6] Despite their low σ_2 values (<5 GM), these compounds were shown to be efficient stains of nucleic-acid-containing organelles in the cytoplasma.[5,6] More recently, higher σ_2 values have been reported for styryl dyes.[7] Water-soluble bis(styrylbenzene) derivatives have been prepared with $\sigma_2 \approx 400$ GM and emission quantum yield of 0.2–0.4.[8,9] Incubation of Hella cells with these dyes resulted in bright emission localized in the plasma membrane with no observable internalization.[8,9] A series of relatively simple carbazole containing pyridinium dyes with σ_2 up to 600 GM in acetonitrile and very good contrast in staining mitochondria were recently reported.[10] One of the best water-soluble nonlinear dyes reported up to date are bicationic fluorene derivatives, with $\sigma_2 \approx 730$ GM and an emission quantum yield of 0.35 in water, which were shown to be selective

Special Issue: Markku Räsänen Festschrift

Received: July 16, 2014
Revised: August 18, 2014

   dx.doi.org/10.1021/jp507095b | J. Phys. Chem. A XXXX, XXX, XXX–XXX

mitochondria markers.[11] Other families of cationic dyes with high σ_2 values have been reported but have not been tested yet as stains for imaging of in vivo cells. Examples of this are (dimethoxyphenyl)ethynyl-methylpyridium based molecules with linear (A^+-π-A^+) structure and σ_2 values of up to 3500 GM.[12,13] Application of these compounds is limited by the low emission quantum yields (<0.1)[13] and low solubility in water. Cationic triphenylamine-based molecules have been recently reported to have both high emission quantum yields (0.70 in methanol) and high TPA cross-section (4150 GM).[14] The water solubility issue could be circumvented to some extent by the use of surfactants at the expense of TPF efficiency, which decreased by a factor of 5.

In this work, a systematic investigation of the photophysics of dipolar and quadrupolar cationic molecules with general D-π-A^+ and D-π-A^+-π-D structure (see Figure 1) is presented, with special emphasis on the TPA properties. The effects of donor strength, conjugation length, and symmetry in the TPA efficiency are analyzed in detail. Single dye/multicolor imaging of living cells is demonstrated for the best nonlinear fluorophore. The intrinsic affinity to DNA exhibited by the symmetric dyes is also addressed.

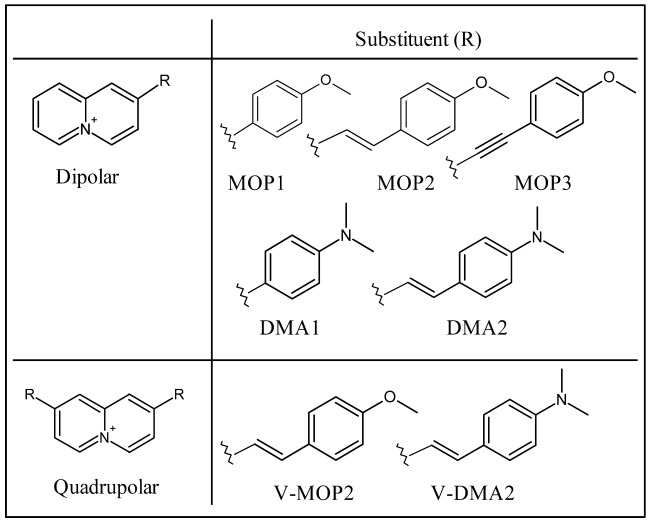

Figure 1. Quinolizinium-based dipolar and quadrupolar V-shaped molecules.

2. EXPERIMENTAL SECTION

2.1. Synthesis. Dipolar compounds **MOP1**, **MOP3**, and **DMA1** were obtained from 2-bromoquinolizinium bromide using different palladium-catalyzed cross-coupling reactions.[15] **MOP1** and **DMA1** were synthesized by the Suzuki–Miyaura coupling reaction using either the appropriate arylboronic acids or alternatively potassium organotrifluoroborates, an efficient reagent, which allow functionalization on quinolizinium under mild conditions with high yields.[16] **MOP3** was obtained by the Sonogashira reaction as previously reported.[17] The Heck reaction on 2-vinyl quinolizinium hexafluorophosphate allowed for the preparation of compounds **MOP2** and **DMA2** with acceptable yields.[18−20] Finally, quadrupolar V-shape chromophores represented by disubstituted quinolizinium derivatives **V-MOP2** and **V-DMA2** were both obtained from 2,8-dimethylquinolizinium bromide by a double Knoevenagel condensation under the same conditions used for the synthesis of the dipolar compounds and following the procedure reported earlier.[17,21,22] A more detailed description of materials, instrumentation, and synthetic procedure as well the NMR spectra of the new compounds (**MOP1**, **MOP2**, **DMA1** and **DMA2**) can be found in the Supporting Information (S1−S5).

2.2. Instrumentation. The linear absorption spectra were recorded either on a Shimadzu UV-3101PC UV−vis−NIR or a JASCO V-540 spectrophotometer. The emission spectra were recorded on a Horiba Jobin Yvon Fluorolog 3−22 spectrofluorimeter. The spectra were recorded in spectroscopic grade methanol using 5 × 5 mm quartz cells. The fluorescence quantum yields were determined using fluorescein in water at pH = 11 (ϕ = 0.92, λ_{em} = 500−600 nm), rhodamine 101 in ethanol (ϕ = 1.0, λ_{em} = 600−700 nm) or quinine sulfate in 0.5 M sulfuric acid (ϕ = 0.546, λ_{em} = 400−500 nm) as standards, depending on the absorption and emission spectra of the quinolizinium derivative.[23,24] The TPA spectra were measured by TPF using fluorescein at pH >11 (**MOP** set) and rhodamine 6G (**DMA** set) in methanol as standards to account for collection efficiency and pulse characteristics.[25] A modified setup that follows closely the one described by Xu and Webb was used to estimate the TPA cross-section in the 710−990 nm region.[26] The TPF was measured within a narrow wavelength bandwidth selected by the H20Vis Jobin Yvon monochromator placed at the entrance of a PMC-100-4 photomultiplyer tube (Becker and Hickl GmbH). The integrated TPF over the entire emission band was extrapolated using the emission spectra corrected by the detector sensitivity. The excitation source was a Ti:sapphire laser (Tsunami BB, Spectra-Physics, 710−990 nm, 1.7 W, 100 fs, 82 MHz). Solutions of 4−60 μM concentration in methanol were used. The two-photon absorption cross-section was calculated from the equation:

$$\sigma_2 = \left(\frac{F_2}{\varphi C n}\right)_q \left(\frac{\varphi C n \sigma_2}{F_2}\right)_{sd} \quad (1)$$

where F_2 stands for fluorescence intensity, ϕ is the one-photon excited fluorescence quantum yield, n refers to the refractive index of the solution, C is the concentration, and q and sd are relative to the synthesized quinolizinium derivatives and the TPA standards, respectively. The emission intensity dependence of the excitation power was checked to be quadratic for all compounds at different wavelengths within the TPA bandwidth. Within each set of compounds the relative error is at most ±20%. However, an uncertainty of ∼50% should be considered when attempting to compare cross-section values obtained with different standards.

The fluorescence lifetimes were measured by the single photon timing technique using the second harmonic of a cavity-dumped DCM dye laser, synchronously pumped by a solid state Nd:YVo4 laser (Vanguard, Spectra Physics) delivering 2W of 532 nm light at 76 MHz repetition rate with a pulse duration of ∼12 ps, as an excitation source. Emission was measured at the magic angle by an Hamamatsu R-2809 MCP photomultiplier. The instrument response functions (∼35 ps fwhm) for deconvolution were generated from scattering dispersions of colloidal silica in water. The fluorescence decays were analyzed by a nonlinear least-squares reconvolution method using the TRFA DP software by SSTC (Scientific Software Technologies Center, Belarusian State University, Minsk, Belarus).

2.3. Cell Staining Procedure and Fluorescence Microscopy Imaging. Human embryonic kidney cells (HEK 293) were cultured in Dulbecco's modified Eagle's

dx.doi.org/10.1021/jp507095b | J. Phys. Chem. A XXXX, XXX, XXX−XXX

medium (DMEM) supplemented with 10% fetal calf serum, 100 IU/mL penicillin, and 100 g/mL streptomycin in a 5% CO_2 incubator at 37 °C. The cells were grown on 1 μ-Slide 8 well uncoated ibidi glass coverslips. Prior to the addition of cells, the chambers were coated with poly-L-lysine for at least 30 min, then each well was washed several times with PBS. The cells were subsequently added to the wells and cultured with DMEM without phenol red for 2 days before each experiment. Cell culture reagents were from Invitrogen Corp. (Carlsbad, CA), and fetal bovine serum (FBS) was from Atlanta Biologicals (Lawrenceville, GA). Solutions of 10^{-4} M concentration of the V-MOP2 dye in methanol were used as stock solutions. Several staining protocols were attempted by changing the **V-MOP2** concentration from 2 to 10 μM, generally by adding a fixed volume of 2 μL of stock solutions with different concentration to 200 μL of culture medium. The incubation periods at 37 °C with 5% CO_2 ranged from 5 to 30 min with and without wash.

The cells were imaged using a laser scanning confocal microscope (Leica TCS-SP5) equipped with an continuous Ar ion laser (458, 465, 488, 496, and 514 nm) and a Ti:sapphire (Spectra-Physics Mai Tai BB, 710−990 nm, 100 fs, 82 MHz). Both confocal and multiphoton imaging are possible using either the Ar ion laser or the Ti:sapphire laser. For fluorescence lifetime imaging (FLIM) a photomultiplyer tube was coupled to the X-port of the microscope and the emission was processed by an SPC board that addresses simultaneously the *xy* location of the collected photons (Becker and Hickl GmbH, PMC-100-4 and SPC-830). The SPCM acquisition software and the lifetime image processing SPCImage software were used. The emitted light was discriminated from the excitation light by a dichroic beamsplitter (Semrock, FF665) and a short pass dichroic filter (Semrock, FF01-680/SP). A 63 × 1.2 N.A. water immersion objective was used. Images were collected with a typical scan rate of 400 Hz per frame.

2.4. Computational Methods. Calculations were done using Gaussian 03.[27] Ground state geometry optimizations were performed in vacuum for the isolated molecules at the B3LYP/6-31++g(2d,2p) level, and frequency calculations were used to ensure that a global minimum was reached. TDDFT calculations were done at the same level of approximation to estimate the Franck−Condon transition energies and the corresponding configuration interaction coefficients, transition dipole moments, and oscillator strengths for one-photon absorption (OPA). To obtain an estimate of the shift of the electronic transitions due to solvent and counterion effects, the geometry optimization and one-photon absorption calculations were also carried out for the ion pair in solvent medium (methanol) using the PCM approximation.[28−30]

The degenerate two-photon transition probabilities for linearly polarized light were calculated for the isolated molecules in vacuum by using the response functions formalism at the B3LYP/6-311+g(2d,2p) level of approximation as implemented in the DALTON program.[31−33] In this approach, the two-photon absorption cross-section is calculated analytically as single residues of the quadratic response functions of the molecular electronic density (keyword TWO-PHOTON). A different basis set was used in the calculation of the TPA properties due to the nonavailability in DALTON of the basis set that had been used in the calculation of the OPA properties. The difference in the transition energies calculated with the two basis sets is within the accuracy of the methods. In general the lower excited states discussed in detail in the manuscript, are predicted within 5 nm (~0.03 eV) by the two basis sets.

3. RESULTS AND DISCUSSION

3.1. Linear Photophysics. The linear absorption and fluorescence spectra of the quinolizinium derivatives in methanol are shown in Figure 2, and the corresponding

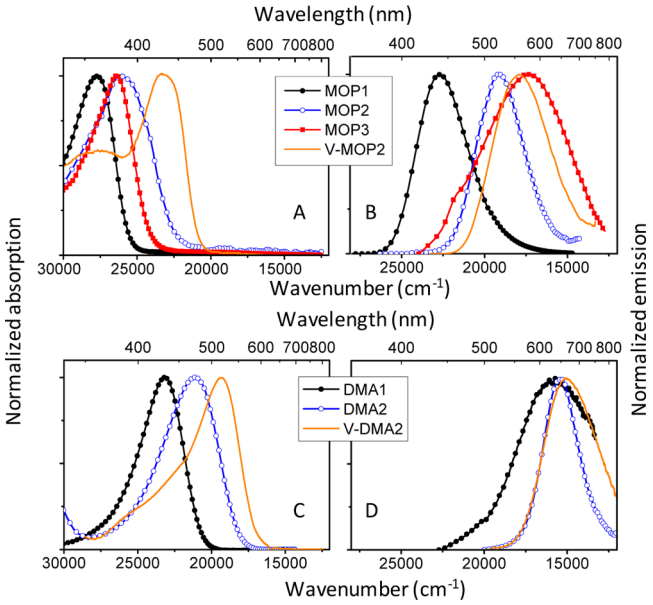

Figure 2. Absorption (A and C) and fluorescence (B and D), spectra of the quinolizinium derivatives in methanol within a μM concentration range. Panels A and B are relative to methoxyphenyl substituted (**MOP**) and panels C and D refer to the dimethylaniline substituted (**DMA**) quinoliziniums derivatives.

absorption and emission maxima are listed in Table 1, together with the fluorescence quantum yields. In both the methoxyphenyl substituted (**MOP** set) and the dimethylaniline substituted (**DMA** set) quinoliziniums the absorption maxima systematically deviate to longer wavelengths with the increasing extent of π-delocalization in the order **MOP1** < **MOP2** ≈ **MOP3** < **V-MOP2** (Figures 2A) and **DMA1** < **DMA2** < **V-DMA2** (Figure 2C).

In the **MOP** set of compounds, the one with the shorter conjugation length (**MOP1**) has an absorption maximum at 361 nm that shifts to 392 and 379 nm for **MOP2** and **MOP3**, appearing at the longest wavelength in **V-MOP2** (432 nm). Table 2 shows the calculated transition energies, oscillator strength, and the contribution of each excitation to the lower energy transitions within the singlet manifold. The isodensity surfaces of the frontier molecular orbitals are shown in Figure 3. Including explicitly the counterion and the solvent does not have a significant effect in the nature of the frontier molecular orbitals (see Figure 3 for the molecules in vacuum and Supporting Information, S6 for the counterion and solvent effect). The calculations in vacuum predict relatively well the observed trend in the transition energies in solution, albeit with a systematic underestimation by 0.4 eV (~60 nm). The stabilization of the polar ground state in the presence of the solvent and counterion leads to a general increase of the vertical transition energies and a better agreement between the calculated and experimental data. This effect is more pronounced in the **MOP** series (0.21 eV average shift between

dx.doi.org/10.1021/jp507095b | J. Phys. Chem. A XXXX, XXX, XXX−XXX

Table 1. Photophysical Properties of the Quinolizinium Derivatives: Maximum Linear Absorption, and Emission Wavelength (λ_{max} OPA and λ_{max} OPE), Maximum Linear Absorption Coefficient (ε), S_0-S_1 Energy Gaps (E_g), Average Fluorescence Lifetime (τ), Nonradiative Deactivation Rate (k_{nr}), Maximum Two-Photon Absorption Wavelength (λ_{max} TPA), Two-Photon Absorption Cross-Section at the Maximum Absorption Wavelength (σ_2), and Emission Quantum Yield (ϕ)

cmpd	λ_{max} OPA (nm)	ε (/10^4) (M^{-1} cm^{-1})	λ_{max} OPE (nm)	E_g[a] (eV)	τ[b](ns)	ϕ[c]	k_{nr}[d](s)	λ_{max} TPA (nm)	σ_{2max}[e](GM)	$\sigma_2\phi$ (GM)
MOP1	361	2.7	437	2.8	3.11	0.76(0)	7.7×10^7	720	70	53
MOP2	392	5.5	517	2.4	0.16	0.03(6)	6.0×10^9	780	270	10
MOP3	379	1.9	574	2.3	0.75	0.02(1)	1.3×10^9	760	60	1
V-MOP2	432	5.4	546	2.2	1.22	0.22(0)	6.4×10^8	760	1140	250
DMA1	432	4.3	608	2.0	0.24	0.00(3)	4.1×10^9	860	160	<1
DMA2	474	5.2	643	1.9	0.12	0.01(8)	8.1×10^9	950	200	4
V-DMA2	518	5.0	650	1.9	0.07	0.00(3)	1.4×10^{10}	880	340	1

[a]Energy gaps approximated by the emission maxima. [b]Average lifetime determined as a $\tau = \Sigma_i a_i \tau_i / \Sigma_i a_i$. [c]Fluorescein in water at pH = 11 (ϕ = 0.92), rhodamine 101 in ethanol (ϕ = 1.0) or quinine sulfate in 0.5 M sulfuric acid (ϕ = 0.546) were used as standards, depending on the absorption and emission spectra of the compound [d]$k_{nr} = (1 - \phi)/\tau$. [e]Measured by TPF using fluorescein in water at pH >11 (**MOP** set) and rhodamine 6G in methanol (**DMA** set) as standards.

calculated and experimental transition energies vs 0.13 eV in the **DMA** set) due to the comparatively larger dipole moments of the compounds in this set. The increase of the vertical transition energies is particularly evident for the transitions with stronger charge-transfer character in the dipolar molecules, such as those involving excitation into the second lowest energy virtual orbital (LUMO + 1 or simply L + 1). Within the **MOP** set, the calculations in vacuum predict that, with the exception of **V-MOP2**, the strongest band in the visible region has significant contributions from two different transitions, $S_0 \rightarrow S_1$ and $S_0 \rightarrow S_2$, where the ground state electron density from the highest energy occupied molecular orbital (HOMO or simply H) is redistributed into the L and L + 1 orbitals, resulting in a net electron density transfer from the donor group to the quinolizinium center (Figure 3). In the presence of the solvent and counterion the two lowest energy electronic transitions become more localized in either the H → L or H→ L + 1 excitation. The particularly broad absorption band of **MOP2** when compared with **MOP1** and **MOP3** (Figure 2) might result from the fact that these two transitions are predicted further apart [38 (46) nm in vacuum (solution)], both having relevant contributions to the absorption band centered at 392 nm [25 (12)% contribution of the H → L + 1 to the total intensity predicted in vacuum (solution)]. For **V-MOP2** the strongest transition, observed at 432 nm and predicted at 519 (477) nm, has a dominant contribution from the H → L transition (Table 2). The shoulder observed at shorter wavelengths (360 nm) is predicted to be a H − 1 → L + 1 ($S_0 \rightarrow S_3$) transition with a calculated peak position at 428 (382) nm and an oscillator strength around 1 (Table 2). The quadrupolar compounds have C_{2v} symmetry and the lower energy $\pi-\pi^*$ excited states belong to either A1 or B2 symmetry, being simultaneously OPA and TPA allowed. Nevertheless, the two bands in the OPA spectrum have predominant contributions from transitions to B_2 excited states, predicted with oscillator strengths one order of magnitude higher than the transitions to the A1 excited state (Table 2). As it will be discussed later, this relationship between the relative intensities of the A1 and B2 excited states is inverted in the TPA spectra.

The main trend in the fluorescence spectra of the **MOP** set of compounds is the red-shift of the band maxima with increasing electronic delocalization (**MOP1** > **MOP2** > **V-MOP2** in Figure 2B). With the exception of **MOP3**, the fluorescence maxima (Table 1) follow a similar trend as the absorption maxima. **MOP3** shows the largest Stokes shift of all the studied compounds (~10000 cm^{-1}) and the fluorescence band appears much broader than the absorption band, which is an indication that the emissive state is different from the Franck−Condon state and it possesses a strong charge-transfer character. This charge-transfer state has the smallest quantum yield of this set of compounds (ϕ = 0.02).

In the **DMA** set, the absorption maxima appear at 432 nm for **DMA1** shifting to longer wavelengths in **DMA2** (474 nm) and **V-DMA2** (518 nm). The corresponding calculated peak positions for the strongest transitions (449, 490, and 591 nm, respectively for **DMA1**, **DMA2**, and **V-DMA2**) are on average underestimated by less than 0.16 eV (~35 nm). The presence of the solvent and counterion reduces the shift between experimental and calculated transition to 0.13 eV, but it does not have a significant effect in the nature of the frontier orbitals (see Figure 3 for the molecules in vacuum and Supporting Information, S6 for the counterion and solvent effect). As mentioned earlier, the strongest effect is that of increasing the energy of the transitions with strong charge-transfer character in the dipolar compounds. This is the case of the 70−100 nm blueshift (0.4−0.5 eV) of the bands predicted in vacuum at 506 and 546 nm in **DMA1** and **DMA2**, respectively (Table 3). Neither of these two transitions is clearly observed in the OPA spectra because they are either weak or convoluted with other transitions. For the compounds in this set, the strongest band in the absorption spectrum is predicted to correspond to a modest redistribution of the electron density from the donor group to the quinolizinium center associated with a H→ L transition (Table 3 and Figure 3). For **DMA1**, the calculation in solution predict that, in addition to the H → L transition (445 nm), also the H → L + 1 (429 nm) contributes to the lowest energy band observed at 432 nm. The shift of only 16 nm between these two bands does not allow for conclusive identifications of their individual contributions in the experimental spectrum. On the other hand, in **DMA2** the broadness of the main absorption band might be explained by the convolution of the H → L and the H → L + 1 transitions separated by about 50 nm. For **V-DMA2** the calculations predict an additional absorption band at 486 nm (H − 1 → L + 1), about 100 nm blueshifted from the main absorption band at 591 nm, that is assigned to the shoulder observed at about 450 nm in Figure 2.

A very modest conjugation length effect is observed in the fluorescence of this set of molecules where the maximum

dx.doi.org/10.1021/jp507095b | J. Phys. Chem. A XXXX, XXX, XXX−XXX

Table 2. Molecular Orbitals Involved in the Lower Energy Electronic Transitions (>300 nm) Predicted by TDDFT at the B3LYP/6-31++g(2d,2p) level for the MOP Set for the Isolated Molecules in Vacuum and for the Ion Pair in Methanol: Orbitals Involved, Percentage Contribution of Each Excitation to the CI Expansion (%),[a] Wavelength of the Transition (nm), Oscillator Strength (f), and Two-Photon Absorption Cross-Section (σ_2)[b]

	expt			isolated in vacuum				ion pair/MeOH		
	λ_{OPA}^{expt} (nm)	$H_n \rightarrow L_m$		λ (nm)	CI	f	σ_2 (GM)	λ (nm)	CI	f
MOP1										
S_1 (A)		0	+1	426	64	0.070	0.4	352	92	0.103
		0	0		30					
S_2 (A)	361	0	0	399	54	0.614	6.7	368	94	0.677
		0	+1		28					
S_3 (A)		−1	0	329	90	0.008				
S_4 (A)		−1	+1	307	92	0.020				
MOP2										
S_1 (A′)		0	0	480	40	0.323	3.4	426	96	1.217
		0	+1		52					
S_2 (A′)	392	0	+1	442	44	0.941	8.4	380	94	0.160
		0	0		38					
S_3 (A′)		−1	0	350	94	0.003	0.1	310	88	0.136
S_4 (A′)		0	+2	319	88	0.063	8.3			
S_5 (A′)		−2	0	313	64	0.143	3.1	305	88	0.014
S_6 (A′)		−1	+1	304	94	0.013	0.6			
MOP3										
S_1 (A′)		0	+1	471	64	0.279	3.8	370	96	0.020
		0	0		30					
S_2 (A′)	379	0	0	452	50	0.832	12.7	411	98	1.230
		0	+1		32					
S_3 (A′)		−1	0	354	96	0.014		307	90	0.098
S_4 (A′)		0	+2	314	62	0.013	2.6			
S_5 (A′)		−1	+1	312	66	0.026	14.5			
		0	+2		28					
S_7 (A′)		−2	0	310	58	0.167	0.6	300	90	0.015
V-MOP2										
S_1 (B_2)	432	0	0	519	84	1.424	2.89	477	100	1.754
S_2 (A_1)		−1	0	472	58	0.030	61.8	421	90	0.092
		0	+1		38					
S_3 (B_2)	360	−1	+1	428	90	1.069	0.7	383	98	0.941
S_4 (A_1)		0	+1	415	48	0.085	75.6	382	88	0.055
		−1	0		26					
S_5 (B_2)		−2	0	342	88	0.003		324	90	0.132
S_6 (A_1)		−3	0	341	92	0.004		318	84	0.001
S_7 (B_2)		−4	0	325	74	0.188	5.2	314	86	0.006
S_8 (B_2)		0	+3	316	94	0.029	0.3	307	74	0.023
S_9 (A_1)		0	+2	309	72	0.064	0.3	311	90	0.070

[a]Calculated as twice the sum of the squares of the expansion coefficients. Only contributions higher than 20% were included. [b]σ_2 was calculated using a different basis set 6-311+g(2d,2p). Only σ_2 values superior to 0.1 GM were included.

emission wavelength shifts from 631 nm to 648 and 660 nm from **DMA1** to **DMA2** and **V-DMA2** (Figure 2D), respectively. Similarly to that of **MOP3**, the emission spectra of **DMA1** and **V-DMA2** suggest that an emissive charge-transfer state different from the Franck−Condon state is responsible for the broad and unstructured emission. The fluorescence quantum yield of **DMA1** and **V-DMA2** (0.003) are one order of magnitude lower than that of **DMA2** (0.018).

The quinolizinium derivatives under study are charged molecules in the ground state, with a charge deficiency in the quinolizinium ring. Because of the stronger electron donor strength of the donor groups in the dimethylaniline substituted quinoliziniums, the **DMA** derivatives are expected to have a lower permanent dipole moment in the ground state, when compared with the **MOP** derivatives. The aniline donor compensates more efficiently the charge deficiency in the quinolizinium cation. Indeed, the dipole moments calculated for the ground state are systematically lower for the **DMA** set [4.37 D (**DMA1**), 5.45 D (**DMA2**), and 0.98 D (**V-DMA2**)] when compared to the corresponding molecules in the **MOP** set [7.05 D (**MOP1**), 8.57 D (**MOP2**), and 5.33 D (**V-MOP2**)]. The dipole moment, which increases from the single-bond-bridged to the double-bond-bridged arrangement in both sets of derivatives, is reduced by the addition of a second donor arm in the V-shaped molecules due to cancellation effects associated with the C_{2v} symmetry of these molecules. This effect is stronger for the quinolizinium derivative substituted with the strongest donor group, where the dipole moment

dx.doi.org/10.1021/jp507095b | J. Phys. Chem. A XXXX, XXX, XXX−XXX

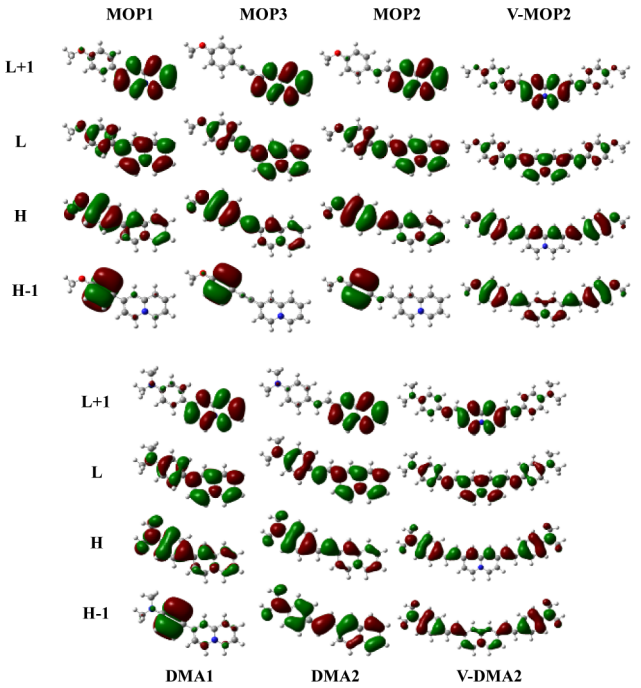

Figure 3. Isodensity surfaces of the frontier molecular orbitals of the methoxyphenyl substituted (**MOP**) and the dimethylaniline substituted (**DMA**) quinolizinium derivatives calculated for the isolated molecules in vacuum.

changes from 5.45 D in **DMA2** to 0.98 D in **V-DMA2**. In the methoxy substituted series, the change goes from 8.57 D in **MOP2** to 5.33 D in **V-MOP2**. A charge transfer from the donor group to the quinolizinium cation in the excited state can lead to a less polar state or ultimately to a reversal of the dipole moment direction. The changes in the dipole moment upon excitation can be followed by analysis of the solvatochromic shifts. As illustrative examples, the solvatochromic shifts of the compounds with larger quantum yields (**MOP1** and **V-MOP2** derivatives) are shown in Figures 4 and 5. These compounds show a hypsochromic shift in absorption (ν_{abs}) and a bathochromic shift in emission (ν_{em}) with increasing solvent orientational polarization function (Δf). These trends show that the permanent dipole moment of the ground and excited states have opposite direction.[34] The fact that the absorption and emission spectra have a mirror image relationship in both molecules (Figures 4A and 5A) indicates that the emissive charge-transfer state is the locally excited state. Thus, the solvatochromic studies can give an estimate of the ratio between the ground and excited state dipole moments from the ratio of the slopes in the ν_{abs} vs Δf (Figures 4C and 5C) and ν_{em} vs Δf (Figures 4B and 5B).[34] For **MOP1**, the ratio is −7.5 showing that the ground state dipole moment is much higher than the excited state, whereas for **V-MOP2**, the ratio is nearly −1 indicating that the states involved in the transition have approximately the same dipole moment and point in opposite direction. Thus, for the strongest transition in the OPA spectrum the change in the permanent dipole moment is stronger in the symmetric quinolizinium. As discussed in the next section, this is a critical factor for the two-photon absorption cross-section.

In general the methoxyphenyl-substituted quinoliziniums show larger quantum yields than the dimethylaniline set (Table 1). The relatively smaller quantum yields in the **DMA** set are believed to be connected to a faster nonradiative deactivation of the excited state in this set of compounds. The nonradiative decay rates (knr), calculated from the emission lifetimes and quantum yield, are shown in Table 1. The dependence of the knr on the energy gaps, also shown in Table 1, can be roughly approximated by an exponential decrease. A graphical representation of the observed trend is shown as Supporting Information (S7). The fluorescence decay curves are complex and generally a sum of three exponentials is needed to achieve a good fit. Short decay components (few picoseconds), associated with the solvent reorganization process after the large charge distribution induced by electronic excitation, have been neglected in the calculation of the average lifetime in Table 1. Solvent relaxation in alcohols is complex with a substantial deactivation occurring within the time resolution of our setup (in the subpicosecond region) and a longer relaxation in the ps region due to hydrogen bond reorganization around the excited molecule.[35,36]

3.2. Two-Photon Absorption. The absolute (σ_2) and effective ($\sigma_2\phi$) TPA cross-section and the TPA maxima ($\lambda_{max\ TPA}$) are listed in Table 1. A simplified three-state model based on the ground state, *g*, and two excited state, *k* and *f*, can be considered, showing that the magnitude of the TPA cross-section is determined by the difference in the permanent electric dipole moments of the ground and final excited state ($\Delta\vec{\mu}_{fg}$), and the transition dipole moments between the ground state and the final excited state and between the final and intermediate excited states according to the expression:[12]

$$\sigma_2(\omega) \propto \langle |\mathbf{M}_{fg}^{(2)}|^2 \rangle \propto \left[\left| \frac{\langle f|\vec{\mu}|k\rangle\langle k|\vec{\mu}|g\rangle}{\omega_{kg} - \omega} \right| \pm \left| \frac{\Delta\vec{\mu}_{fg}\langle f|\vec{\mu}|g\rangle}{\omega} \right| \right]^2 \quad (2)$$

where $\mathbf{M}_{fg}^{(2)}$ is the two-photon transition matrix element and ω is the photon energy in a degenerated two-photon absorption process.

For centrosymmetric molecules, $\Delta\vec{\mu}_{fg}$ is vanishingly small and the second term, known as the dipolar term, has a negligible contribution to the overall two-photon transition probability. In addition, due to the mutual exclusion principle associated with the parity selection rule, the $S_0 \rightarrow S_1$ transition is usually one-photon allowed and two-photon forbidden.[4,12,37] Thus, in centrosymmetric molecules, the lowest energy two-photon allowed transition is expected at higher energies when compared to the lowest energy one-photon allowed transition ($\lambda_{maxTPA} < 2\lambda_{maxOPA}$).

On the other hand, for the lowest energy *f* excited state of most noncentrosymmetric molecules the dipolar terms is dominant, because the intermediate *k* state lies necessarily in the higher energy region and the energy denominator in the three-state term is large.[38] Thus, the lowest energy TPA-allowed state is the same as the lowest OPA state, both dependent on the transition dipole moment between the ground state and the final state. In this case, the lowest energy band in the TPA spectrum appears at exactly twice the energy of the lowest energy transition in the OPA spectrum ($\lambda_{maxTPA} \approx 2\lambda_{maxOPA}$). This is clearly shown in Table 1 where λ_{maxTPA} corresponds to twice the value of λ_{maxOPA} for all the dipolar compounds. As an illustrative example, the TPA and OPA spectra of the dipolar **MOP2** and **DMA2** compounds are shown in Figure 6B,D, featuring mainly the lowest energy transition.

dx.doi.org/10.1021/jp507095b | J. Phys. Chem. A XXXX, XXX, XXX−XXX

Table 3. Molecular Orbitals Involved in the Lower Energy Electronic Transitions (>300 nm) Predicted by TDDFT at the B3LYP/6-31++g(2d,2p) Level for the DMA Set for the Isolated Molecules in Vacuum and for the Ion Pair in Methanol: Orbitals Involved, Percentage Contribution of Each Excitation to the CI Expansion (%),[a] Wavelength of the Transition (nm), Oscillator Strength (f), and Two-Photon Absorption Cross-Section (s_2)[b]

	expt			isolated in vacuum				ion pair/MeOH		
	λ_{OPA}^{expt} (nm)	$H_n \rightarrow L_m$		λ (nm)	CI	f	σ_2 (GM)	λ (nm)	CI	f
DMA1										
S_1 (A)		0	+1	506	82	0.023	0.3	429	0.482	66
		0	0							34
S_2 (A)	432	0	0	449	82	0.833	6.6	445	0.433	66
		0	+1							32
S_3 (A)		0	+2	334	98	0.016	0.7	307	0.016	84
S_4 (A)		−1	0	318	90	0.001	0.1	299	0.118	82
DMA2										
S_1 (A′)	474	0	0	490	46	1.207	1.8	499	1.202	96
		0	+1		28					
S_2 (A′)		0	+1	546	66	0.182	7.5	449	0.218	94
		0	0		26					
S_3 (A′)		0	+2	350	92	0.056	0.1	315	0.011	66
S_4 (A′)		−1	0	337	34	0.132	0.2	328	0.298	74
		−2	0		42					
S_5 (A′)		−2	0	336	52	0.076	0.2	308	0.001	58
		−1	0		30					
S_6 (A′)		−1	+1	312	80	0.036	5.2			
V-DMA2										
S_1 (B2)	518	0	0	591	98	1.495	3.6	561	1.868	100
S_2 (A1)		−1	0	542	60	0.026	75.3	498	0.088	86
		0	+1		40					
S_3 (B2)	450	−1	+1	486	96	1.105	0.8	447	0.844	98
S_4 (A1)		0	+1	460	56	0.132	92.5	439	0.116	86
		−1	0		40					
S_5 (B2)		−2	0	358	76	0.265	2.9	346	0.241	86
S_6 (B2)		0	+3	354	94	0.010	137.0	330	0.010	52
		−1	+2							26
S_7 (A1)		0	+2	345	84	0.105	3.3	346	0.102	90
S_8 (B2)		−4	0	341	90	0.002	4.3	325	0.006	48
S_9 (A1)		−5	0	330	62	0.002	0.5	330	0.003	60
		−3	0		28					
S_{10} (A1)		−1	+3	330	86	0.010	48.7			

[a]Calculated as twice the sum of the squares of the expansion coefficients. Only contributions higher than 20% were included. [b]s_2 was calculated using a different basis set 6-311+g(2d,2p). Only s_2 values superior to 0.1 GM were included.

The shape of the TPA spectrum need not coincide with that of the OPA spectrum. For excited states other than the lowest energy state, both terms in eq 2 should be considered. The interplay between the product of transition dipole moments in eq 2, which becomes smaller with increasing excitation energy due to the expected smaller transition dipole moments between the ground state and excited states of increasing energy, and the so-called resonance enhancement effects, associated with ω approaching ω_{kg} with increasing excitation energy, will determine the relative TPA intensity of higher energy excited states. The relevance of higher energy states to the TPA of the quadrupolar **V-MOP2** and **V-DMA2** compounds is evidenced by the blueshift between the energy of the strongest transitions in the OPA and in TPA spectra (~0.4 eV for both **V-MOP2** and **V-DMA2** corresponding to $\lambda_{maxTPA} - 2\lambda_{maxOPA}$ values of 104 nm in **V-MOP2** and 156 nm in **V-DMA2**) shown in Figure 6A,C. In addition to this stronger absorption, a weaker band appears at lower energies in the TPA spectra of **V-MOP2**, coincident with twice the wavelength of the OPA maxima. Observation of this shoulder is not possible for **V-DMA2** because of the limitations of our excitation source.

The calculations of the two-photon transition matrix element performed on the basis of the single residue of the quadratic response function provide a detailed insight into the nature of the states involved in the TPA process. Tables 2 and 3 list the calculated TPA cross sections for the **MOP** and **DMA** set of compounds. Comparison of the calculated TPA and OPA spectra in vacuum for the dipolar **MOP2** and **DMA2** with those of the corresponding quadrupolar analogues is shown in Figure 7. For the dipolar molecules, the calculations predict that the strongest two-photon transitions coincide with the one-photon transitions (Figure 7B,D). Thus, in agreement with the experimental data (Figure 6B,D), the TPA spectra follow the linear absorption spectra when shifted by the energy of the absorbed photon. For the quadrupolar molecules, the calculation predicts two strong bands in the 600−1200 nm region corresponding to the $S_0 \rightarrow S_2$ (H-1→L) and $S_0 \rightarrow S_4$ (H→L+1) transitions, both with A_1 symmetry. Within our observation window, only the lowest energy bands can be

dx.doi.org/10.1021/jp507095b | J. Phys. Chem. A XXXX, XXX, XXX−XXX

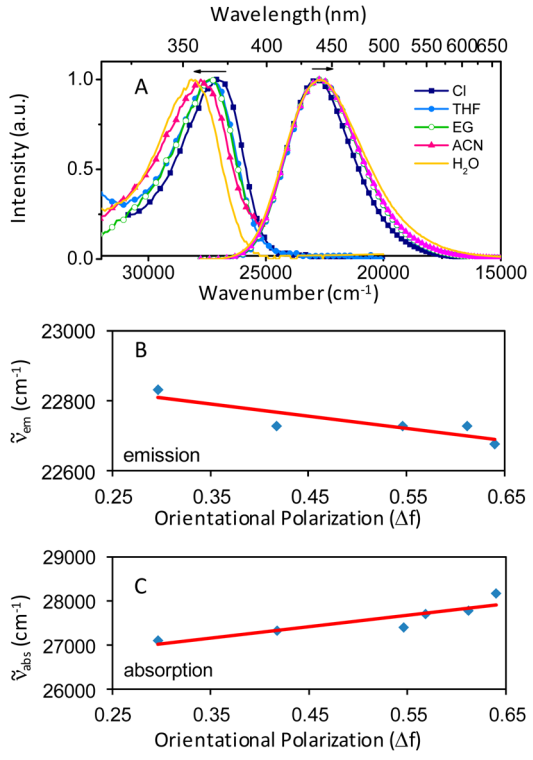

Figure 4. Solvatochromic effect in the spectra of **MOP1** in chloroform (Cl), tetrahydrofuran (THF), ethylene glycol (EG), acetonitrile (ACN), acetone and water (H_2O): absorption and emission spectra (A), emission (B), and absorption (C) maxima as a function of the orientational polarization function of the solvent (Δf). The linear fits shown in each plot correspond to $\nu_{em} = -344.8\Delta f + 22911$ and $\nu_{abs} = 2593.8\Delta f + 26246$.

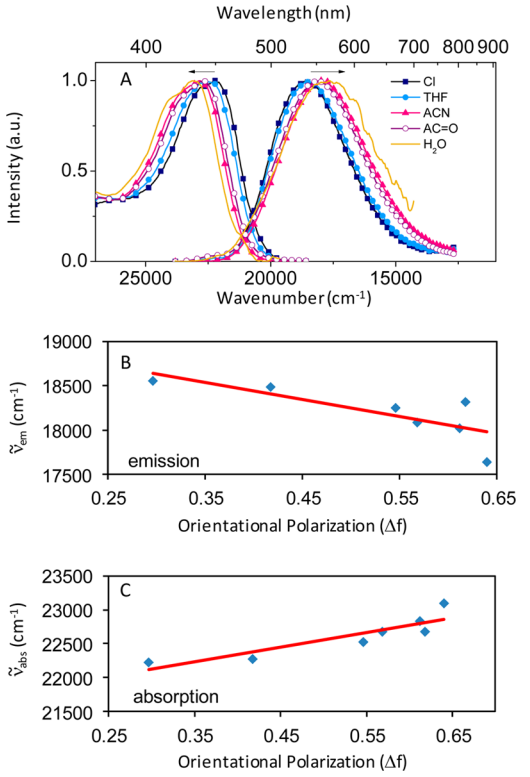

Figure 5. Solvatochromic effect in the spectra of **V-MOP2** in chloroform (Cl), tetrahydrofuran (THF), ethylene glycol (EG), acetonitrile (ACN), acetone and water (H_2O). Absorption and emission spectra (A), emission (B) and absorption (C) maxima as a function of the orientational polarization function of the solvent (Δf). The linear fits shown in each plot correspond to $\nu_{em} = -1935.9\Delta f + 19214$ and $\nu_{abs} = 2166.4\Delta f + 21469$.

observed in the spectra of each compound. According to the calculation, the observed TPA bands at 760 and 880 nm are assigned to the transitions predicted at 472 nm (λ_{TPA} = 1038 nm) and 541 nm (λ_{TPA} = 1082 nm), respectively for **V-MOP2** and **V-DMA2**. Similarly to the OPA spectra, the transition energies observed in the TPA spectra are underestimated by the calculations in vacuum by 0.3−0.4 eV. Noteworthy, the observed bands in the OPA spectra, previously assigned to the B_2 symmetry transitions $S_0 \rightarrow S_1$ (H → L) and $S_0 \rightarrow S_2$ (H − 1 → L + 1), are predicted to have TPA cross sections one order of magnitude lower when compared to the A_1 symmetry transitions. Nevertheless, in the TPA spectrum of **V-MOP2** (Figure 6C) the weaker band at 862 nm is assigned to the B_2 transition observed in the OPA spectrum at 432 nm. These results configure a quasi-mutual exclusion rule between the A_1 and B_2 symmetry and translate into a blueshift of the TPA maxima of the quadrupolar molecules with respect to the corresponding OPA bands as shown by both the experimental spectra in Figure 6A,C and the calculated spectra in and Figure 7A,C. A similar observation has been reported for cruxiform-shaped compounds with C_{2v} symmetry based on tetrakis-(phenylethynyl)benzene.[39]

For both the **MOP** and **DMA** set of compounds, increasing the conjugation length by introduction of a double bond between the donor and acceptor groups increases the TPA cross-section due to an increase of the static dipole moments. The TPA cross-section increases by a factor of 3.6 from **MOP1** to **MOP2** and by 1.3 from **DMA1** to **DMA2**. The highest TPA values are those of the quadrupolar V-shape molecules (1140 GM for **V-MOP2** and 340 GM for **V-DMA2**). Noteworthy, is the fact that the introduction of one more donor arms in **V-MOP2** with respect to **MOP2** increases the TPA cross-section by a factor of 4. This nonadditive effect, also known as cooperative enhancement,[40] shows that the electronic correlation between the two arms plays a role in the nonlinear absorption. A simple model as the one developed by Moreno et al.,[41] relating the TPA cross-section with the energy of the excited states in a three level system and the number of effective electrons, results in an enhancement factor of 2.5 between **MOP2** and **V-MOP2**. This factor is only slightly larger than the additive effect of doubling the number of dipolar branched. The transition dipole moments must be explicitly considered to account for a nonadditive effect as a result of a non-negligible coherent interaction between branches. Indeed, the TPA calculations using the quadratic response function predict a nonadditive enhancement of a factor of 7. In general, the calculated TPA cross sections are about 1 order of magnitude lower as compared to the experimental values. Nevertheless, the relative values provide a reasonable estimation within the **MOP** compounds. **VMOP2** is predicted to have a 5 to 10 times larger cross-section as compared to the dipolar molecules in the **MOP** set, which agrees with the observed 4 to 17 times larger cross-section.

The TPA cross-section shows an additive trend in the **DMA** set. We note that within each set of compounds the TPA cross-section was determined using the same standard as a reference, which means that the relative values should be quite reliable.

dx.doi.org/10.1021/jp507095b | J. Phys. Chem. A XXXX, XXX, XXX−XXX

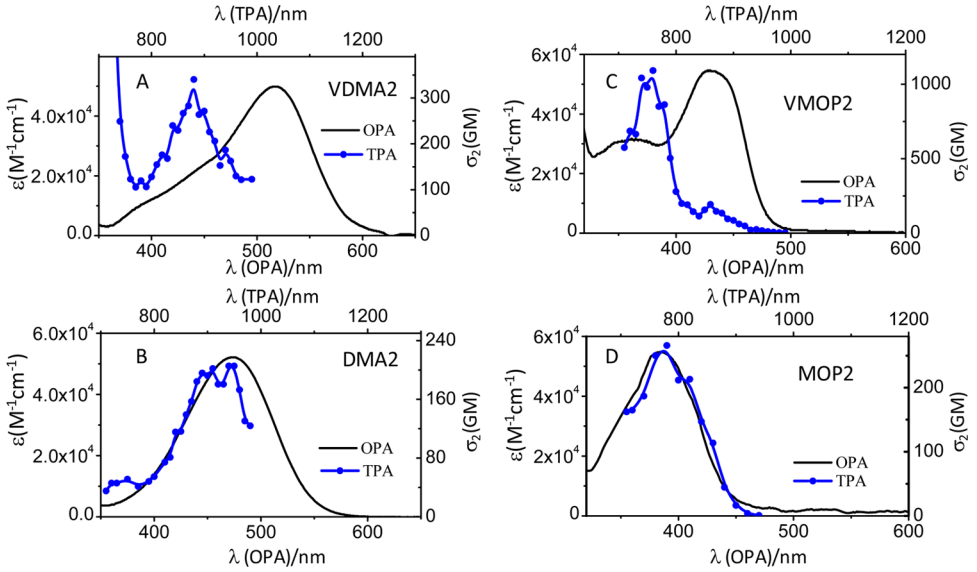

Figure 6. Comparison of OPA (straight black line) and TPA (blue line with dots) spectra for **V-DMA2** (A), **DMA2** (B), **V-MOP2** (C), and **MOP2** (D). Note that the lower wavelength axis in each plot is relative to the OPA spectra while the upper wavelength is relative to the TPA spectra.

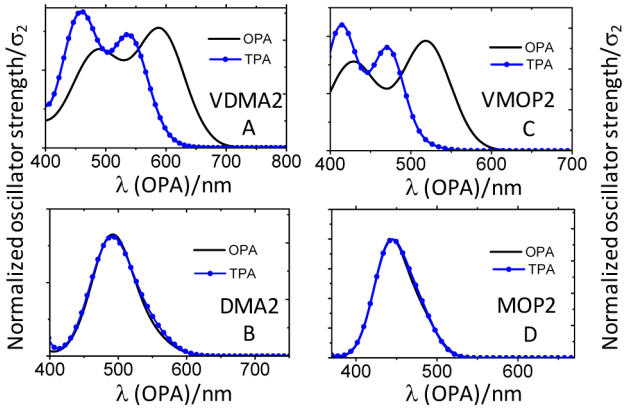

Figure 7. Comparison of calculated OPA (straight black line) and TPA (dotted blue line) spectra for isolated **V-DMA2** (A), **DMA2** (B), **V-MOP2** (C), and **MOP2** (D) in vacuum. The TPA spectra are plotted as a function of half the excitation wavelength.

The quantum yields of **V-DMA2** and **DMA1**, which can also be a major source of error in the determination of the TPA cross-section, have been determined using **DMA2** as a reference. This procedure is estimated to lead to relative values of the TPA in the **DMA** set that should be accurate within ±20%. In the **DMA** set, the agreement between the experimental and calculated TPA cross sections is also worse. A possible explanation is that even though the calculated transition energies for the **DMA** set are on average within 0.2 eV of the experimental values, the shifts between the observed and calculated values for the quadrupolar molecule are larger by more than a factor of 2 when compared with that of the dipolar molecules (0.29 eV for **V-DMA2** and 0.1 eV for the dipolar molecules). This could be an indication that the electronic correlation effects in the quadrupolar molecule, which relate to the nonadditive trend, are overestimated in the **DMA** set. In the **MOP** set the shift between the experimental and calculated data is also larger for the quadrupolar molecules, but it approaches that of the dipolar ones (0.43 for **V-MOP2** and 0.33−0.36 for **MOP1** and **MOP2**).

Experimentally, there is no clear trend as to which donor is the best in terms of TPA cross sections. From Table 1, a comparison of analogue compounds shows that **MOP1** has a σ_2 lower than **DMA1** by a factor of 2, **MOP2** and **DMA2** have similar σ_2 values, and **V-MOP2** has a σ_2 three times higher than that of **V-DMA2**. This is in agreement with the fact that the TPA cross-section of analogous **MOP** and **DMA** compounds are not predicted to be significantly different (see Tables 2 and 3). Nevertheless, owing to its larger fluorescence quantum yield, **V-MOP2** has a considerably higher nonlinear brightness. The stability of the **V-MOP2** was found to be comparable to fluorescein under excitation at 400 nm (∼10% drop in emission upon 30 min excitation with a fluence of 20 mW/cm^2 using the lamp of the spectrofluoremeter).

3.3. Lifetime Imaging. In view of the large TPA cross-section of **V-MOP2**, evaluation of its performance as a dye for in vivo imaging was investigated earlier.[21] **V-MOP2** was found to successfully permeate the living cell membrane. Even though the staining protocol was not exhaustively optimized, it was possible, at reduced concentrations (2 μM) and relatively short incubation times (30 min), to obtain a higher degree of selectivity of the dye toward the cytoplasm. Within the cytoplasm, the positively charged **V-MOP2** appears to accumulate in vesicular cell organelles that are mostly mitocondria.[21] A similar staining pattern is observed in other positively charged dyes such as Rhodamine 123 and styryl dyes with spermine-like linkage.[6,42]

On the other hand, increasing the concentration of the dye in the incubation medium leads to a clear penetration of the dye also in the nucleus. Figure 8 compares fluorescence intensity and lifetime images of HEK cells stained with **V-MOP2**. Interestingly, fluorescence lifetime imaging allows a discrimination between the different cell compartments (cytoplasm, nuclear membrane, or nucleus) without the need for costaining protocols using several dyes that distribute selectively in specific compartment. Thus, the fluorescence lifetime of **V-MOP2** allows the acquisition of a multicolour image using a single dye. In the lifetime image, the longer lifetimes (∼1.6 ns) are shown in blue and belong to the **V-MOP2** within the nucleus, while the shorter lifetimes (∼0.7 ns) appear in orange and

dx.doi.org/10.1021/jp507095b | J. Phys. Chem. A XXXX, XXX, XXX−XXX

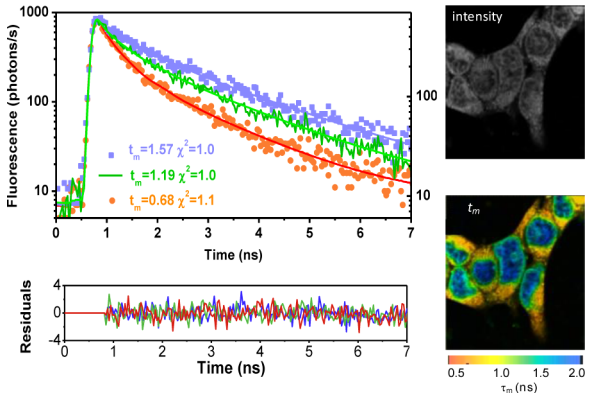

Figure 8. Fluorescence lifetime imaging of HEK cells stained with **V-MOP2**. The 60 μm × 60 μm lifetime image was collected with a resolution of 256 × 256 pixels under excitation at 740 nm. Analysis of the decay lifetime was made with a binning of 5 × 5. The intensity and lifetime images are shown in the right panels. The left panel shows typical fluorescence decay curves of the dye in different cell compartments and the corresponding residuals: longer lifetimes in the nucleus (1.57 ns), shorter lifetimes in the cytoplasm (0.68), and intermediate lifetimes in the nuclear membrane (1.19 ns). Lifetime, χ^2, and residuals were obtained from fitting the fluorescence decay to a double exponential.

correspond to **V-MOP2** accumulated in cytoplasmatic organelles. The frontier green region with intermediate lifetimes (~1.2 ns) is assigned to the nuclear membrane.

As discussed in greater detail in the following section, the different lifetimes measured for **V-MOP2** in the different cell compartments are related to the interaction of the dye with DNA. In an aqueous solution the average lifetime of the dye increases from 0.4 to 1.3 ns upon the addition of DNA sodium salt (~10 bp equiv). Thus, **V-MOP2** is mostly present as a free dye in the cytoplasm where it has the lowest lifetime (0.7 ns), while its interaction with the DNA in the nucleus results in a significantly longer lifetime (1.6 ns). The intermediate lifetimes that mark the nuclear membrane are believed to be the result of the colocalization of free and complexed dye within the 1.2 μm × 1.2 μm region corresponding to the pixel size of the lifetime image after a binning of 5 × 5.

3.4. Interaction with DNA. Similarly to positively charged styryl dyes and recently reported cationic tryphenilamine based dyes, both **V-MOP2** and **V-DMA2** were found to interact with DNA.[5−7] In aqueous solutions the quinolizinium derivatives have a low fluorescence quantum yield and a solubility on the μM range. Interaction with DNA leads to a marked increase of their fluorescence (Figure 9A,B) due to two factors: solubilization of the otherwise aggregated dye upon interaction with the anionic phosphodiester groups along the DNA backbone and a decrease of the nonradiative rate. Taking **V-MOP2** as an example, the addition of ~10 bp equiv of DNA sodium salt to a μM solution of the dye in 0.05 M tris-HCl buffer, pH 8.0, increases the quantum yield by a factor of ~7 (from 0.03 to 0.2) and the average lifetime increases by a factor of ~3 (from 0.4 to 1.3 ns); thus, the nonradiative rate decreases by a factor of 4 and the radiative rate increases by a factor of 2. The decrease of the nonradiative rate upon interaction with DNA can be related to protection of the solute molecules from the solvent provided by intercalation in the double helix and/or to an effect of hindered internal rotation.

In addition, a decrease by 1 order of magnitude is observed in the absorption of **V-MOP2** in water when compared to

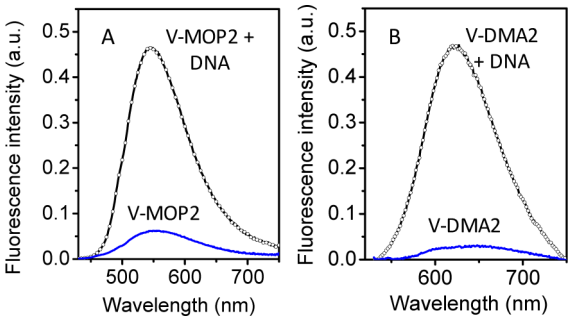

Figure 9. The effect of the addition of 80 μM bp of DNA sodium salt from salmon test on the fluorescence intensity of **V-MOP2** (A) and **V-DMA** (B) in 0.05 M Tris-HCl buffer at pH 8.0. The solid line correspond to the dyes alone, while the open circles refer to the dyes in the presence of DNA.

methanol, accompanied by only minor shifts (<10 nm) on the absorption and emission band maxima. A rough estimation on how much the absorption cross-section is affected by the solvent can be done on the basis of the Strickler−Berg relationship,[43] which relates the radiative deactivation rate with the integrated absorption cross-section, the reciprocal of the mean emission wavenumber, and the square of the refractive index. The ratio of the radiative rates determined from the emission lifetimes (1 ns in methanol and 0.4 ns in water) and the quantum yields (0.22 in methanol and 0.03 in water) anticipates a decrease in the absorption cross-section by a factor of 2.5 in water, but neither the mean emission wavenumber nor the refractive index change significantly with the solvent. Thus, the decrease by a factor of 10 in the absorption in water can have an additional contribution from the formation of nonemissive aggregates, the solubilization of which occurs upon interaction with the DNA.

4. CONCLUSION

Through the systematic study of the photophysics of dipolar and quadrupolar quinolizinium derivatives of general D-π-A^+ and D-π-A^+-π-D structure with dimethylaniline and methoxyphenyl donor group we can conclude the following:

(i) the methoxyphenyl substituted quinoliziniums show larger fluorescence quantum yields than the dimethylaniline set, which ultimately determines their success as fluorophores;
(ii) the quantum yields of the quinolizinium derivatives increase with a decrease of the nonradiative decay rate, which depends on the S_1−S_0 energy gap;
(iii) the best linear fluorophore is **MOP1** with a fluorescence quantum yield of 0.76;
(iv) the best nonlinear fluorophore is the symmetric methoxyphenyl derivative **V-MOP2** with a quantum yield of 0.22 and a TPA cross-section of ~1140 GM, which results in an effective TPA cross-section of 245 GM (roughly 5 times larger than the effective TPA cross-section **MOP1**, the best linear fluorophore);
(v) incubation of HEK cells with the best nonlinear fluorophore (**V-MOP2**) leads to internalization and lifetime imaging allows to discriminate between molecules localized in different cell compartments;
(vi) in aqueous solution, interaction of the quadrupolar molecules (**V-MOP2** and **V-DMA2**) with DNA leads to an increase in the fluorescence emission.

dx.doi.org/10.1021/jp507095b | J. Phys. Chem. A XXXX, XXX, XXX−XXX

■ ASSOCIATED CONTENT

Supporting Information

Detailed description of materials, instrumentation and synthetic procedure, NMR spectra of the new compounds (**MOP1**, **MOP2**, **DMA1**, and **DMA2**), frontier molecular orbital of the ion pair in methanol, and nonradiative rate dependence on the energy gaps. This material is available free of charge via the Internet at http://pubs.acs.org.

■ AUTHOR INFORMATION

Corresponding Author

*E-mail:ermelinda.macoas@tecnico.ulisboa.pt. Tel:(351)218 419 206.

Present Address

⊥G.M.: Departamento de Química Analítica, Química Física e Ingeniería Química, Universidad de Alcalá, 28871, Alcalá de Henares, Madrid, Spain.

Notes

The authors declare no competing financial interest.

■ ACKNOWLEDGMENTS

The authors acknowledge financial support from the Spanish Ministerio de Economía y Competitividad (Project CTQ2011-24715), the Portuguese Fundação para a Ciência e a Tecnologia (Projects PTDC/CTM-POL/114367/2009, RECI/CTM-POL/0342/2012) and a grant from the Universidad de Alcalá (TC).

■ REFERENCES

(1) He, G. S.; Tan, L.-S.; Zheng, Q.; Prasad, P. N. Multiphoton Absorbing Materials: Molecular Designs, Characterization, and Applications. *Chem. Rev.* **2008**, *108*, 1245−1330.

(2) Konig, K. Multiphoton Microscopy in Life Sciences. *J. Microsc.* **2000**, *200*, 83−104.

(3) Diaspro, A.; Chirico, G.; Collini, M. Two-Photon Fluorescence Excitation and Related Techniques in Biological Microscopy. *Q. Rev. Biophys.* **2005**, *38*, 97−166.

(4) Pawlicki, M.; Collins, H. A.; Denning, R. G.; Anderson, H. L. Two-Photon Absorption and the Design of Two-Photon Dyes. *Angew. Chem., Int. Ed.* **2009**, *48*, 3244−3266.

(5) Tokar, V. P.; Losytskyy, M. Y.; Ohulchanskyy, T. Y.; Kryvorotenko, D. V.; Kovalska, V. B.; Balanda, A. O.; Dmytruk, I. M.; Prokopets, V. M.; Yarmoluk, S. M.; Yashchuk, V. M. Styryl Dyes as Two-Photon Excited Fluorescent Probes for DNA Detection and Two-Photon Laser Scanning Fluorescence Microscopy of Living Cells. *J. Fluoresc.* **2010**, *20*, 865−872.

(6) Yashchuk, V. M.; Kudrya, V. Y.; Losytskyy, M. Y.; Valentyna, P. T.; Yarmoluk, S. M.; Dmytruk, I. M.; Prokopets, V. M.; Kovalska, V. B.; Balanda, A. O.; Kryvorotenko, D. V.; et al. The Optical Biomedical Sensors for DNA Detection and Imaging Based onTwo-Photon Excited Luminescent Styryl Dyes: Phototoxic Influence on the DNA. *Proc. SPIE* **2007**, *6796*, 67960M.

(7) Jędrzejewskaa, B.; Krawczyk, P.; Pietrzak, M.; Gordel, M.; Matczyszyn, Katarzyna; Samoć, M.; Cysewski, P. Styryl Dye Possessing Donor-π-Acceptor Structure—Synthesis, Spectroscopic and Computational Studies. *Dyes Pigm.* **2013**, *99*, 673−685.

(8) Nag, O. K.; Nayak, R. R.; Lim, C. S.; Kim, I. H.; Kyhm, K.; Cho, B. R.; Woo, H. Y. Two-Photon Absorption Properties of Cationic 1,4-Bis(styryl)benzene Derivative and its Inclusion Complexes with Cyclodextrins. *J. Phys. Chem. B* **2010**, *114*, 9684−9690.

(9) Woo, H. Y.; Liu, B.; Kohler, B.; Korystov, D.; Mikhailovsky, A.; Bazan, G. C. Solvent Effects on the Two-Photon Absorption of Distyrylbenzene Chromophores. *J. Am. Chem. Soc.* **2005**, *127*, 14721−14729.

(10) Liu, X.; Sun, Y.; Zhang, Y.; Zhao, N.; Zhao, H.; Wang, G.; Yu, X.; Liu, H. A Series of Carbazole Cationic Compounds with Large Two-Photon Absorption Cross Sections for Imaging Mitochondria in Living Cells with Two-Photon Fluorescence Microscopy. *J. Fluoresc.* **2011**, *21*, 497−506.

(11) Tani, S.; Nakagawa, K.; Honda, T.; Saito, H.; Suzuki, Y.; Kawamata, J.; Uchida, M.; Sasaki, A.; Kinjo, M. Fluorescence Imaging of Mitochondria in Living Cells Using a Novel Fluorene Derivative with a Large Two-Photon Absorption Cross-Section. *Curr. Pharm. Biotechnol.* **2012**, *13*, 2649−2654.

(12) Kamada, K.; Iwase, Y.; Sakai, K.; Kondo, K.; Ohta, K. Cationic Two-Photon Absorption Chromophores with Double- and Triple-Bond Cores in Symmetric/Asymmetric Arrangements. *J. Phys. Chem. C* **2009**, *113*, 11469−11474.

(13) Iwase, Y.; Kamada, K.; Ohta, K.; Kondo, K. Synthesis and Photophysical Properties of New Two-Photon Absorption Chromophores Containing a Diacetylene Moiety as the Central pi-Bridge. *J. Mater. Chem.* **2003**, *13*, 1575−1581.

(14) Fang, Z.; Zhang, X. H.; Lai, Y. H.; Liu, B. Bridged Triphenylamine Based Molecules with Large Two-Photon Absorption Cross Sections in Organic and Aqueous Media. *Chem. Commun.* **2009**, *8*, 920−922.

(15) Fozard, A.; Jones, G. Quinolizines. 5. Synthesis and Properties of Some Hydroxyquinolizinium Salts. *J. Chem. Soc.* **1963**, 2203−2209.

(16) Cañeque, T.; Cuadro, A. M.; Alvarez-Builla, J.; Vaquero, J. J. Efficient Functionalization of Quinolizinium Cations with Organotrifluoroborates in Water. *Tetrahedron Lett.* **2009**, *50*, 1419−1422.

(17) Garcia, D.; Cuadro, A. M.; Alvarez-Builla, J.; Vaquero, J. J. Sonogashira Reaction on Quinolizium Cations. *Org. Lett.* **2004**, *6*, 4175−4178.

(18) Barchin, B. M.; Valenciano, J.; Cuadro, A. M.; Alvarez-Builla, J.; Vaquero, J. J. Use of the Stille Coupling Reaction on Heteroaromatic Cations: Synthesis of Substituted Quinolizinium Salts. *Org. Lett.* **1999**, *1*, 545−547.

(19) Garcia-Cuadrado, D.; Cuadro, A. M.; Barchin, B. M.; Nunez, A.; Caneque, T.; Alvarez-Builla, J.; Vaquero, J. J. Palladium-Mediated Functionalization of Heteroaromatic Cations: Comparative Study on Quinolizinium Cations. *J. Org. Chem.* **2006**, *71*, 7989−7995.

(20) Miyadera, T.; Iwai, I. Studies on Quinolizinium Salts. I. Syntheses of Quinolizinium + 1-, 2-, 3-, + 4-Methylquinolizinium Bromides. *Chem. Pharm. Bull.* **1964**, *12*, 1338−1343.

(21) Maçôas, E.; Marcelo, G.; Pinto, S.; Caneque, T.; Cuadro, A. M.; Vaquero, J. J.; Martinho, J. M. G. A V-Shaped Cationic Dye for Nonlinear Optical Bioimaging. *Chem. Commun.* **2011**, *47*, 7374−7376.

(22) Sato, K.; Okazaki, S.; Yamagishi, T.; Arai, S. The Synthesis of Azoniadithia[6]helicenes. *J. Heterocyc. Chem.* **2004**, *41*, 443−447.

(23) Eaton, D. F. Reference Materials for Fluorescence Measurement. *Pure Appl. Chem.* **1988**, *60*, 1107−1114.

(24) Magde, D.; Wong, R.; Seybold, P. G. Fluorescence Quantum Yields and Their Relation to Lifetimes of Rhodamine 6G and Fluorescein in Nine Solvents: Improved Absolute Standards for Quantum Yields. *Photochem. Photobiol.* **2002**, *75*, 327−334.

(25) Makarov, N. S.; Drobizhev, M.; Rebane, A. Two-Photon Absorption Standards in the 550−1600 nm Excitation Wavelength Range. *Opt. Express* **2008**, *16*, 4029−4047.

(26) Xu, C.; Webb, W. W. Measurement of Two-Photon Excitation Cross Section of Molecular Fluorophores with Data From 690 to 1050 nm. *J. Opt. Soc. Am. B* **1996**, *13*, 481−491.

(27) Frisch, M. J.; Trucks, G. W.; Schlegel, H. B.; Scuseria, G. E.; Robb, M. A.; Cheeseman, J. R.; Montgomery, J. A., Jr.; Vreven, T.; Kudin, K. N.; Burant, J. C.; Millam, J. M.; Iyengar, S. S.; Tomasi, J.; Barone, V.; Mennucci, B.; Cossi, M.; Scalmani, G.; Rega, N.; Petersson, G. A.; Nakatsuji, H.; Hada, M.; Ehara, M.; Toyota, K.; Fukuda, R.; Hasegawa, J.; Ishida, M.; Nakajima, T.; Honda, Y.; Kitao, O.; Nakai, H.; Klene, M.; Li, X.; Knox, J. E.; Hratchian, H. P.; Cross, J. B.; Bakken, V.; Adamo, C.; Jaramillo, J.; Gomperts, R.; Stratmann, R. E.; Yazyev, O.; Austin, A. J.; Cammi, R.; Pomelli, C.; Ochterski, J. W.; Ayala, P. Y.; Morokuma, K.; Voth, G. A.; Salvador, P.; Dannenberg, J. J.; Zakrzewski, V. G.; Dapprich, S.; Daniels, A. D.; Strain, M. C.;

Farkas, O.; Malick, D. K.; Rabuck, A. D.; Raghavachari, K.; Foresman, J. B.; Ortiz, J. V.; Cui, Q.; Baboul, A. G.; Clifford, S.; Cioslowski, J.; Stefanov, B. B.; Liu, G.; Liashenko, A.; Piskorz, P.; Komaromi, I.; Martin, R. L.; Fox, D. J.; Keith, T.; Al-Laham, M. A.; Peng, C. Y.; Nanayakkara, A.; Challacombe, M.; Gill, P. M. W.; Johnson, B.; Chen, W.; Wong, M. W.; Gonzalez, C.; Pople, J. A. *Gaussian 03*, revision C.02; Gaussian, Inc.: Wallingford, CT, 2004.

(28) Miertus, S.; Scrocco, E.; Tomasi, J. Electrostatic Interaction of a Solute with a Continuum—A Direct Utilization of Abinitio Molecular Potentials for the Prevision of Solvent Effects. *Chem. Phys.* **1981**, *55*, 117−129.

(29) Barone, V.; Cossi, M.; Tomasi, J. A New Definition of Cavities for the Computation of Solvation Free Energies by the Polarizable Continuum Model. *J. Chem. Phys.* **1997**, *107*, 3210−3221.

(30) Mennucci, B.; Tomasi, J. Continuum Solvation Models: A New Approach to the Problem of Solute'S Charge Distribution and Cavity Boundaries. *J. Chem. Phys.* **1997**, *106*, 5151−5158.

(31) Mcclain, W. M. Excited State Symmetry Assignment through Polarized 2-Photon Absorption Studies of Fluids. *J. Chem. Phys.* **1971**, *55*, 2789−2796.

(32) Monson, P. R.; Mcclain, W. M. Polarization Dependence of 2-Photon Absorption of Tumbling Molecules with Application to Liquid 1-Chloronaphthalene and Benzene. *J. Chem. Phys.* **1970**, *53*, 29−37.

(33) *Dalton, a Molecular Electronic Structure Program*, release Dalton2011; SURFsara: Amsterdam, The Netherlands, 2011; http://daltonprogram.org.

(34) Valeur, B.; Berberan-Santos, M. N. *Molecular Fluorescence*; 2nd ed.; Wiley-VCH Verlag GmbH: Weinheim (Germany), 2012.

(35) Horng, M. L.; Gardecki, J. A.; Papazyan, A.; Maroncelli, M. Subpicosecond Measurements of Polar Solvation Dynamics—Coumarin-153 Revisited. *J. Phys. Chem.* **1995**, *99*, 17311−17337.

(36) Adhikary, R.; Mukherjee, P.; Kee, T. W.; Petrich, J. W. Excited-State Intramolecular Hydrogen Atom Transfer and Solvation Dynamics of the Medicinal Pigment Curcumin. *J. Phys. Chem. B* **2009**, *113*, 5255−5261.

(37) Ohta, K.; Kamada, K. Theoretical Investigation of Two-Photon Absorption Allowed Excited States in Symmetrically Substituted Diacetylenes by ab Initio Molecular-Orbital Method. *J. Chem. Phys.* **2006**, *124*, 124303.

(38) Ohta, K.; Antonov, L.; Yamada, S.; Kamada, K. Theoretical Study of the Two-Photon Absorption Properties of Several Asymmetrically Substituted Stilbenoid Molecules. *J. Chem. Phys.* **2007**, *127*, 084504.

(39) Ohta, K.; Yamada, S.; Kamada, K.; Slepkov, A. D.; Hegmann, F. A.; Tykwinski, R. R.; Shirtcliff, L. D.; Haley, M. M.; Salek, P.; Gel'mukhanov, F.; et al. Two-Photon Absorption Properties of Two-Dimensional pi-Conjugated Chromophores: Combined Experimental and Theoretical Study. *J. Phys. Chem. A* **2011**, *115*, 105−117.

(40) Chung, S. J.; Kim, K. S.; Lin, T. H.; He, G. S.; Swiatkiewicz, J.; Prasad, P. N. Cooperative Enhancement of Two-Photon Absorption in Multibranched Structures. *J. Phys. Chem. B* **1999**, *103*, 10741−10745.

(41) Moreno, J. P.; Kuzyk, M. G. Fundamental Limits of the Dispersion of the Two-Photon Absorption Cross Section. *J. Chem. Phys.* **2005**, *123*, 194101.

(42) Johnson, L. V.; Walsh, M. L.; Chen, L. B. Localization of Mitochondria in Living Cells with Rhodamine-123. *Proc. Natl. Acad. Sci. U.S.A.* **1980**, *77*, 990−994.

(43) Strickler, S. J.; Berg, R. A. Relationship between Absorption Intensity and Fluorescence Lifetime of Molecules. *Spectrochim. Acta* **1962**, *18*, 1358−1358.